

Showcasing research from Professor Michinao Hashimoto's laboratory, Engineering Product Development, Singapore University of Technology and Design, Tampines, Singapore.

Microfluidic paper-based analytical soft actuators (μ PAC)

Soft actuators have developed over the last decade for diverse applications including industrial machines and biomedical devices. Integration of chemical sensors would be beneficial, but there have been limited devices to achieve such sensing capabilities. A soft actuator has finally met with a paper-based microfluidic device! Called the microfluidic paper-based analytical soft actuator (μ PAC), μ PAC serves as a unique actuating platform for chemical sensing. Highlighting the unique capability of μ PAC, we demonstrated the local detection of pH on the curved target surface. Artwork design by Dr. Koki Yoshida.

Image reproduced by permission of Koki Yoshida from *Lab Chip*, 2025, **25**, 2364.

As featured in:



See Michinao Hashimoto *et al.*,
Lab Chip, 2025, **25**, 2364.


 Cite this: *Lab Chip*, 2025, 25, 2364

Microfluidic paper-based analytical soft actuators (μPAC)†

 Koki Yoshida,^{ab} Masahiro Tanakinoue,^{ac}
 Hiroaki Onoe ^d and Michinao Hashimoto ^{*b}

Soft actuators have developed over the last decade for diverse applications including industrial machines and biomedical devices. Integration of chemical sensors with soft actuators would be beneficial in analyzing chemical and environmental conditions, but there have been limited devices to achieve such sensing capabilities. In this work, we developed a thin-film soft actuator integrated with a paper-based chemical sensor, termed a microfluidic paper-based analytical soft actuator (μPAC). μPAC consists of (1) a silicone thin film with a 3D-printed pneumatic chamber and (2) a cellulose paper. This cellulose paper offers dual functions: the strain-limiting layer of a soft actuator and the substrate for the chemical sensor for a paper-based analytical device (μPAD). We characterized the design parameters of the actuators—namely, (1) thickness of silicone thin film, (2) chamber length, and (3) Young's modulus of silicone thin film—to evaluate the actuation performance. These characterizations suggested that the cellulose paper served as a suitable self-straining layer of the actuator, making μPAC a chemical sensor that can actuate simultaneously. Highlighting the unique capability of μPAC, we demonstrated the local detection of pH on the curved target surface. Overall, this research demonstrated the rapid fabrication of actuating chemical sensors with a unique design by combining soft actuators and μPAD, enabling chemical sensing on various surface topologies by dynamically making conformal contact.

 Received 17th July 2024,
 Accepted 12th November 2024

DOI: 10.1039/d4lc00602j

rsc.li/loc

Tribute to George Whitesides

Happy 85th birthday, George. When I joined graduate school in 2003, I aspired to become a theoretical scientist. Something unexpected happened, and I ended up doing experiments in the Whitesides group. This serendipity has shaped my career. The experience in the group allowed me to become a handyperson without limiting my curiosity to any specific discipline. It is not about being interdisciplinary or cross-disciplinary, but rather about creating new disciplines that did not exist before. Pioneering a discipline is a challenging but worthwhile goal, and I greatly benefited from seeing many excellent examples set by my colleagues in the early stages of my scientific career. In the lab, I worked closely with my senior colleague, Piotr Garstecki, on droplet microfluidics. I appreciated the philosophy of *simple solutions* in the group. I brought the idea of *simple solutions* to my research group, continuing to develop technologies that others can use. The topic we explored in this paper is built on two *simple* technologies—paper-based microfluidics and soft actuators—from the Whitesides group. With this, I hope to illustrate how I have continued to enjoy exploring science and engineering, building on the foundation laid in your group. Happy birthday, George, and many more to come!

Michinao Hashimoto

1. Introduction

This work developed actuable chemical sensors, termed a microfluidic paper-based analytical soft actuator (μPAC). Soft actuators have been developed over the last decade due to their flexibility and compliance with applications for industrial machines, biomedical devices, and wearable devices.^{1–5} Unlike conventional rigid counterparts operated by electrical inputs, soft grippers can be controlled by heat,⁶ light,⁷ air pressure,⁸ or liquid displacement.^{9,10} Such characteristics offer various advantages, including conformability, complex motion, and reduced energy consumption. In particular, pneumatic soft grippers, consisting

^a Research Center for Autonomous Systems Materialogy, Institute of Integrated Research, Institute of Science Tokyo, Japan

^b Pillar of Engineering Product Development, Singapore University of Technology and Design, 8 Somapah Road, 487372, Singapore. E-mail: hashimoto@sutd.edu.sg; Tel: +65 6499 4867

^c Department of Computer Science, Institute of Science Tokyo, 4259 Nagatsuta-cho, Midori-ku, Yokohama, Kanagawa 226-8502, Japan

^d Department of Mechanical Engineering, Keio University, 3-14-1 Hiyoshi, Kohoku-ku, Yokohama, 223-8522, Japan

† Electronic supplementary information (ESI) available. See DOI: <https://doi.org/10.1039/d4lc00602j>

of pneumatic chambers and microchannels, are widely used due to their simple control without mechanical components.^{11–14} Pneumatic chambers typically consist of soft elastomers combined with different Young's modulus components to achieve anisotropic deformation.^{15,16} Different approaches—such as embedding paper,¹⁷ reinforcing with fibers (e.g., polyaramid fibers^{18,19} and cotton threads²⁰), increasing the number of layers,²¹ knitting,²² and regulating balloon inflation^{23,24}—have been used to achieve asymmetric strain, leading to programmed deformation of the actuator. The deformation can be designed by the geometry and the arrangement of materials comprising the actuator;^{23,25} different modes of actuation have been demonstrated, such as expanding,¹⁷ contracting,¹⁵ twisting,²⁶ and bending.²⁷ Soft actuators are often fabricated by casting the silicone elastomer in the negative molds. Polydimethylsiloxane

(PDMS) and Ecoflex are widely used silicone elastomers due to their processability, biocompatibility, and stretchability. Recent advances in 3D printing have enabled alternative ways to fabricate soft actuators. Stereolithography and extrusion 3D printing have been utilized to pattern various materials to create microchannels and chambers.^{28–32} These technologies are applied to the fabrication of soft actuators, including milli-meter scale pneumatic soft grippers by multi-material digital light processing (DLP)-based 3D printing³³ and biodegradable soft actuators by fused deposition modeling (FDM) printing.²⁰

More recently, the integration of sensors with soft actuators has been demonstrated to self-sense the condition of the actuator.^{34–36} Successful demonstrations are shown for sensing proximity¹⁴ and own strain.³⁷ The capability to sense the state of the soft actuators offers precise control for the actuation.

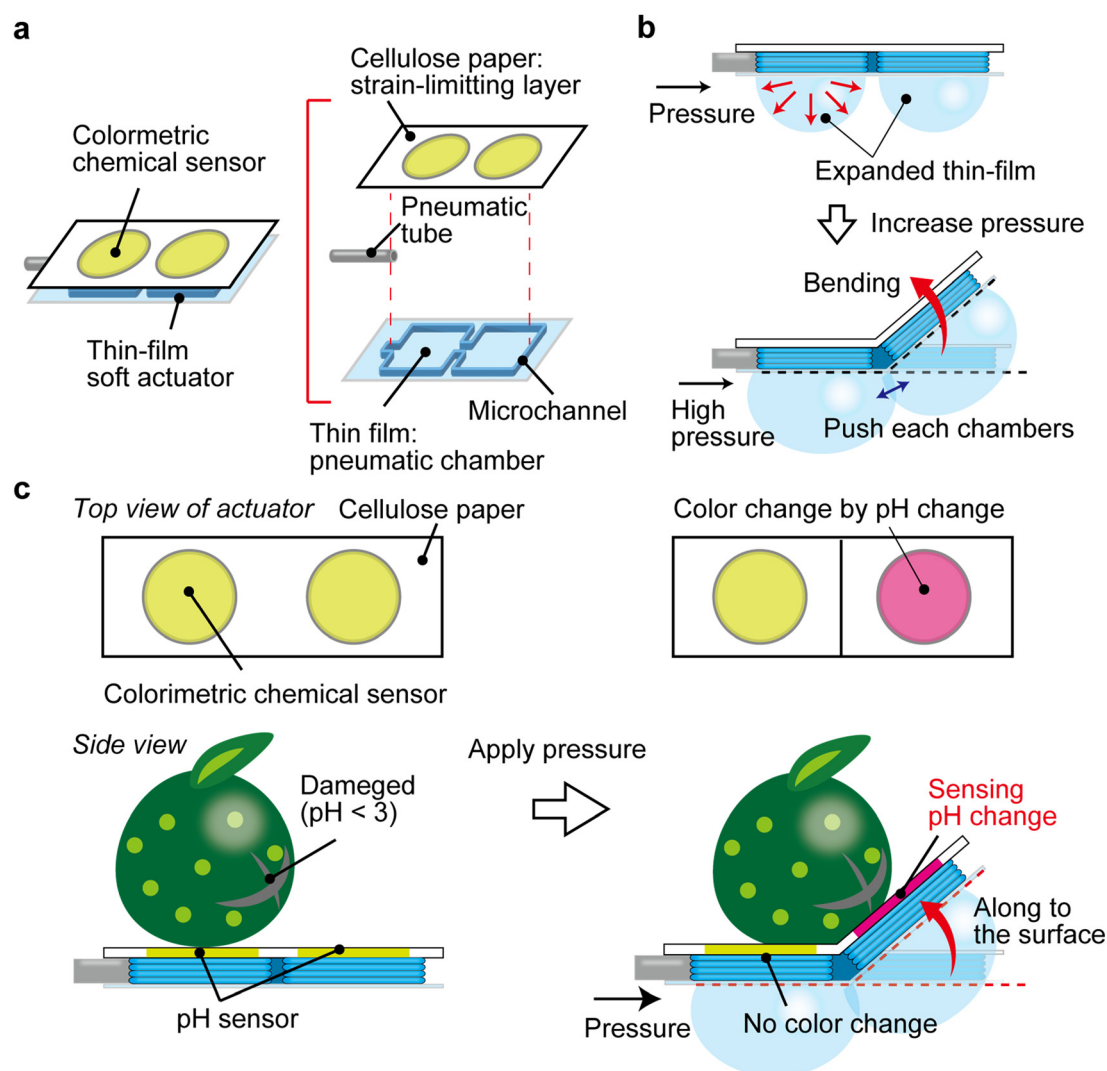


Fig. 1 Schematic illustration of a microfluidic paper-based analytical soft actuator (μ PAC). (a) Illustration of μ PAC. μ PAC consists of (1) cellulose paper and (2) silicone sealant printed on a silicone thin film. A silicone tube (i.e., pneumatic tube) is inserted to the microchannel to apply pressure. (b) Expansion of the pneumatic chambers. The pneumatic chambers are expanded by the pressure applied through the pneumatic tube. The expansion of the chambers leads to the bending motion. (c) Integration of chemical sensors with the soft actuator. The paper-based substrate is placed as a strain-limiting layer of the soft actuator. This layer simultaneously serves as a substrate for chemical sensing, which conformally contracts with the surface where the soft actuator is in contact. As an example, colorimetric pH sensing by μ PAC is illustrated.

Electrical sensing of the surrounding conditions (*e.g.*, tactile sensing of the surface) has also drawn remarkable attention.^{14,37,38} On the other hand, integrating chemical sensors with soft actuators is essential to identify the chemical and environmental conditions, including pH and material concentrations, which will find various practical applications in agriculture and healthcare. Hydrogel with biomolecules (*e.g.*, DNA and enzyme) or synthetic bacteria have been used as soft and compliant materials for surface chemical sensing because hydrogel can permeate molecules, withholding the sensing elements.^{39–42} Alternatively, porous materials (such as cellulose papers) have been widely explored as a substrate for colorimetric chemical sensing.^{43,44} Paper-based chemical sensors are primarily constructed by immersing colorimetric sensor inks into microchannels made with molten wax.^{45,46} Despite its desired characteristics, however, the direct integration of cellulose paper substrates with soft actuators to perform chemical sensing has not been explored.

Here, we present a thin-film soft actuator integrated with a paper-based chemical sensor, termed a microfluidic paper-based analytical soft actuator (μ PAC, Fig. 1a). μ PAC consisted of (1) silicone-based microchannels as pneumatic chambers and (2) a wax-based chemical reservoir. Crucially, both components can be digitally patterned by DIW 3D printing. The paper substrate offered dual functions: the strain-limiting layer of a soft actuator and the substrate for a microfluidic paper-based analytical device (μ PAD). The silicone chambers were expanded by pneumatic pressure, leading to the deformation of μ PAC in a similar manner to conventional pneumatic actuators (Fig. 1b). We performed parametric studies for the bending behaviors of μ PAC by changing the geometric parameters: chamber size, thickness, and Young's modulus. Then, the repeated actuation of the μ PAC was demonstrated. μ PAC can deform and make conformal contact with a target object to detect surface chemical conditions, illustrated by colorimetric pH sensing (Fig. 1c). Overall, we developed a unique design of actuatable paper-based chemical sensors by combining a paper-based fluidic system with an elastomeric actuator in a single device, termed μ PAC. The paper substrate is designed as part of the actuator that can move and conform to the surface being analyzed. We envisage that the unique capability of μ PAC could lead to diverse applications. For example, integrating μ PAC into a soft robotic gripper for agricultural and food products may enable on-site detection of chemical contaminants during handling.^{47–49} μ PAC could also be used for sampling of the physiological lumen when mounted on the tip of an endoscope.⁵⁰ Additionally, μ PAC might be used to capture environmental samples by the integration with aerial robots.^{51,52} These application scopes highlight the versatility of μ PAC across different disciplines, from healthcare to environmental monitoring.

2. Experimental design

2.1. Selection of materials

The objective of this research is to investigate ways to integrate a soft actuator with a chemical sensor. We selected

the cellulose paper as a substrate of the soft actuator due to its desirable properties: (1) permeable to aqueous solutions, (2) not stretchable yet flexible, and (3) porous. The permeability to aqueous solutions enables the handling of aqueous samples and chemical sensing as demonstrated in μ PAD. Cellulose papers have also been widely used as *origami* or *kirigami* structures to create deformable structures, allowing reversible deformation required for the actuation. Lastly, the cellulose paper is porous, which enables the physical integration of composite materials. In this research, the printed silicone elastomer was mechanically interlocked with a paper substrate to achieve a stable bonding between the elastomer and the substrate. The molten wax was also printed on the paper to create hydrophobic regions on the paper, which was essential for creating analytical domains for aqueous samples.

2.2. Selection of fabrication methods

Conventional pneumatic actuators have complex three-dimensional (3D) designs, and they combine materials with different stiffness for actuation. In this work, we aimed to simplify the fabrication process for rapid manufacturing. We proposed an alternative design of a soft actuator that could be fabricated by DIW printing. In our design, 3D-printed square microchambers were sandwiched between pre-fabricated thin-film substrates with different stiffness: a silicone thin film and a cellulose paper. The different stiffness is crucial for bending motion (ESI S1,† Fig. S1). Fabrication of soft actuators was achieved by printing the outlines of two-dimensional (2D) microfluidic chambers.⁵³ This approach reduces the materials and time required to create microchambers in comparison with molding. Crucially, μ PAD can be also fabricated by DIW printing, which is also an essential component of the device we intend to achieve. Overall, due to the design of the actuator, and the applicable printing materials (*i.e.*, silicone resin and wax), DIW printing was used to perform the fabrication of μ PAC.

3. Results and discussion

3.1. Bending characteristics of μ PAC

Fig. 1 illustrates the concept of the current research. A proposed μ PAC have pneumatic chambers with a square length (7.5 mm or 10 mm) (Fig. 2a). The microchannel connecting pneumatic chambers were 2 mm in length and 2 mm in width. For fabricating the pneumatic chamber with microchannels, the silicone sealant was printed by a DIW printer on the thin-film elastomeric substrates (Ecoflex 0-10 and Ecoflex 00-30, Fig. 2b). Young's modulus of the cured Ecoflex 00-10 and Ecoflex 00-30 were 41 kPa,⁵⁴ 169.4 kPa,⁵⁵ respectively. The silicon tube (outer diameter: 1 mm) was placed on the printed silicone sealant microchannel. The additional silicone sealant was then printed on the silicone tube to immobilize them. After that, the cellulose paper was set on the printed microchannel. The printed silicone sealant was solidified overnight together with the cellulose paper,

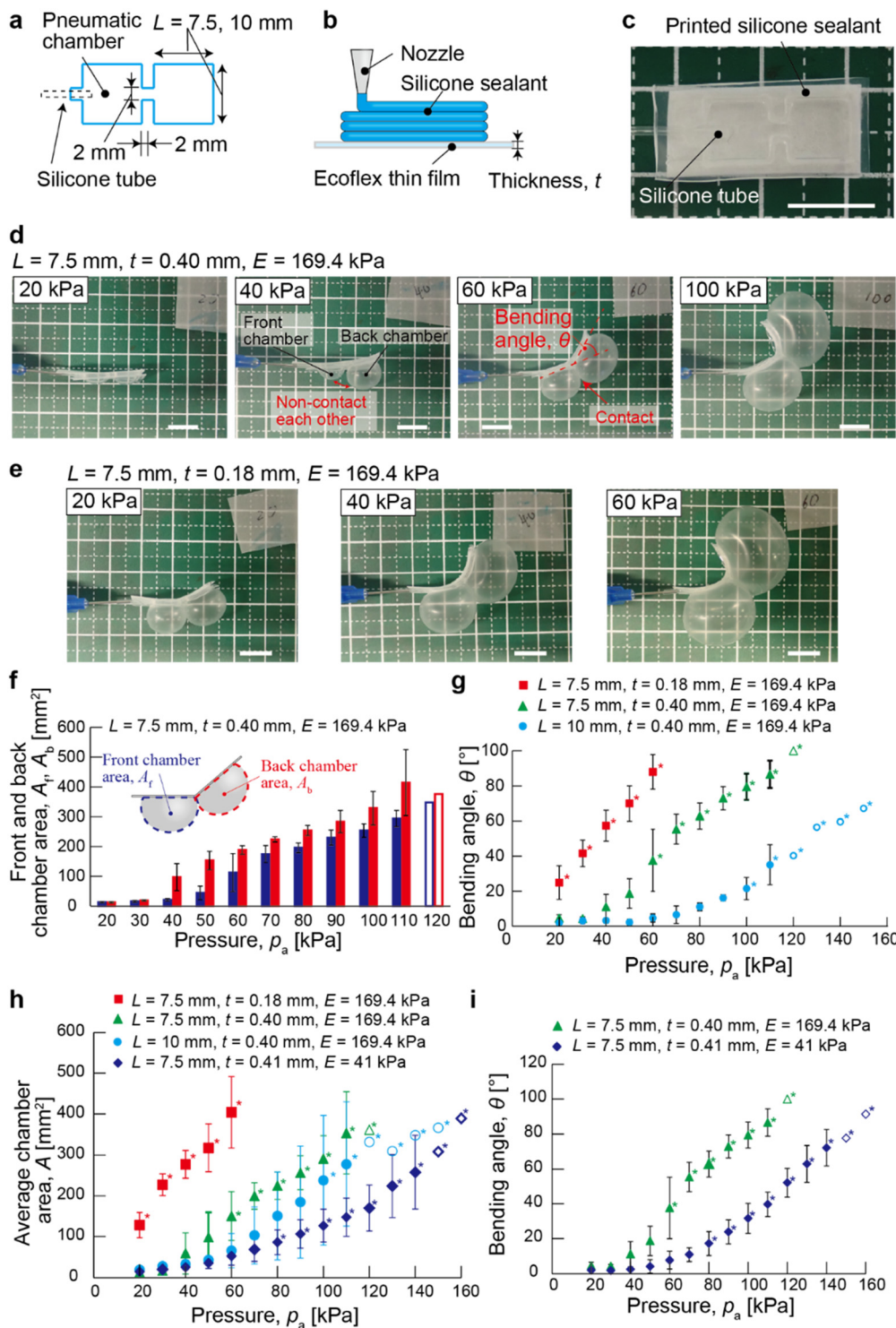


Fig. 2 Characterization of the bending motion of μ PAC. (a) Design of the microchamber of μ PAC. (b) Schematic illustration of the printing of the silicone sealant, and the thickness of the thin film (t). (c) Photograph showing a fabricated μ PAC. (d and e) Photographs showing the bending behavior of μ PAC with increasing pressure (p_a), with different thickness of the film: (d) 0.40 mm and (e) 0.18 mm. (f) Plot showing the areas of the front chamber (A_f) and the back chamber (A_b) with respect to pressure (p_a). (g) Plot showing the bending angle of μ PAC (θ) with respect to pressure (p_a), (h) plot showing the average chamber areas of μ PAC (A) with respect to pressure (p_a). (i) Plot showing the bending angles of μ PAC (θ) with respect to pressure (p_a). The physical parameters of μ PAC (L , t , E) are indicated in each plot. In all plots, unfilled marks suggest the measurement was performed less than triplicate ($n = 3$). The asterisk (*) suggests when two pneumatic chambers are in contact. Scale bars: 10 mm.

promoting the integration of the printed sealant with the cellulose paper (Fig. 2c). We created the actuator consisting of two square chambers in the front and the back to study the bending behaviors.

To actuate μ PAC, the pneumatic pressure was applied through the silicone tube using an air dispenser at a constant pneumatic pressure. The elastomeric chambers expanded and reached a steady state due to the contact pressure applied to the chamber (Fig. 2d). The expanded chambers maintained the shape, suggesting the outflow of the gas through the cellulose paper can be compensated by the inflow of the gas to the chamber. When the two adjacent pneumatic chambers became sufficiently large to push against each other, μ PAC exhibited the bending motion. The degree of actuation of μ PAC was affected by altering the thickness of the silicone thin film (Fig. 2e).

To perform a detailed characterization of bending behaviours, we altered the pneumatic pressure (p_a), the thickness of the thin silicone film (t), the chamber length (L) and Young's modulus of the elastomer (E). The pneumatic pressure (p_a) was increased from 20 kPa in increments of 10 kPa, repeating the process until the elastomeric layer of μ PAC was ruptured. When applying the pneumatic pressure ($p_a = 20$ kPa) to μ PAC with $L = 7.5$ mm, $t = 0.40$ mm, and $E = 169.4$ kPa, the actuator hardly bent (with the bending angle, $\theta = 4.6 \pm 2.0^\circ$). In this case, the pneumatic chambers slightly expanded (with the cross-sectional chamber area $A = 12.8 \pm 2.0$ mm²), and did not push each other (Fig. 2d, left and 2f). When the pneumatic pressure increased to $p_a = 40$ kPa, the pneumatic chamber expanded (Fig. 2d). In this chamber design, the cross-sectional area of the back chamber, $A_b = 97.4 \pm 45.7$ mm², was larger than the front chamber area, $A_f = 21.2 \pm 4.2$ mm² (Fig. 2f). When increasing the pneumatic pressure the pneumatic to $p_a = 60$ kPa, the pneumatic chambers further expanded and pushed each other ($A_f = 112.7 \pm 63.8$ mm², $A_b = 188.4 \pm 14.6$ mm²), leading to bending of μ PAC with $\theta = 37.6 \pm 17.7^\circ$. The chamber area and bending angle were increased as the pneumatic pressure increased (Fig. 2f and g, green triangles). The bending angle of μ PAC (θ) ranged from $4.6 \pm 2.0^\circ$ to $87.0 \pm 7.8^\circ$ when the pneumatic pressure (p_a) ranged from 20 kPa to 110 kPa (Fig. 2f, green triangles). The silicone thin film with $t = 0.40$ mm withstood the pressure up to $p_a \sim 110$ kPa; the same silicone thin film in the chamber burst at $P_a \sim 120$ kPa. These results suggested that bending behavior largely depended on the expansion of the pneumatic chambers resulting in mutual pushing. It is also worth noting that the silicone thin film burst before the adhesive detached, suggesting that the printed silicone sealant tightly bonded both sides of the films (*i.e.*, the silicone thin film and the cellulose paper).

Next, we used the thinner silicone film ($t = 0.18$ mm) to evaluate the bending characteristics of μ PAC ($L = 7.5$ mm and $E = 169.4$ kPa). At the reduced pneumatic pressure ($p_a = 20$ kPa), this design of μ PAC expanded with average chamber area, $A = 128.2 \pm 31.1$ mm² and bent with $\theta = 24.9 \pm 9.5^\circ$

(Fig. 2e, left and 2h, red square). The bending angle of the μ PAC (θ) ranged from $24.9 \pm 9.5^\circ$ to $88.0 \pm 9.8^\circ$ when the pneumatic pressure (p_a) ranged from 20 kPa to 60 kPa (Fig. 2g, red squares). Similar to the design of μ PAC with $t = 0.40$ mm, the back chamber was more readily expanded than the front chamber (details in ESI† S2, Fig. S2). While the pneumatic chamber was readily expanded by the applied pressure, the thin film was broken at $P_a \sim 70$ kPa. The maximum bending angle and the average chamber area were $\theta = 88.0 \pm 9.8^\circ$ and $A = 404.7 \pm 87.2$ mm². These values were similar to the device with the larger film thickness ($t = 0.40$ mm; $\theta = 87.0 \pm 7.8^\circ$, $A = 354.1 \pm 100.5$ mm²). These results suggested that the bending behavior of μ PAC was dependent on the expansion of the pneumatic chambers. The responsiveness of μ PAC to the applied pressure can be controlled by the thickness of the silicone thin film. In addition, the thickness of the silicone thin film did not influence the maximum bending angle for the two devices we studied ($t = 0.18$ mm and 0.40 mm) while the tolerances of the pneumatic chamber were different.

Then, we changed the side length of the square chamber to $L = 10$ mm ($t = 0.40$ mm, $E = 169.4$ kPa). A relatively small pneumatic pressure ($p_a < 90$ kPa) did not bend the actuator ($\theta < 20^\circ$). The average chamber area increased slightly due to the expansion of the back chamber, but the actuator did not bend because the two chambers did not contact (Fig. 2g, sky blue circles, 2h, sky blue circles, and S3†). The maximum bending angle was $\theta = 35.1 \pm 11.4^\circ$ ($p_a = 110$ kPa), which was much smaller than the actuator with $L = 7.5$ mm ($\theta = 86.7 \pm 7.8^\circ$). These results indicated that the increased chamber size caused large contrasts in the expansion behaviors between the front chamber and back chamber, resulting in less bending of μ PAC. The maximum chamber area ($A = 277.7 \pm 152.4$ mm²) was also smaller than μ PAC with $t = 0.40$ mm and $L = 7.5$ mm because of the imbalance of expansion. The maximum pneumatic pressure before the rupture of the silicone thin film remained as $p_a = 110$ kPa (that was the same as the actuator with $t = 0.40$ mm and $L = 7.5$ mm), indicating that the chamber size did not influence the tolerance of the thin film actuator.

Lastly, we examined the bending behavior of μ PAC using a thin film with a low Young's modulus ($E = 41$ kPa) and the same dimensions ($L = 7.5$ mm and $t = 0.41$ mm). In this case, the chambers in the actuator required high pneumatic pressure to expand. The average chamber area ranged from 14.7 ± 2.0 mm² to 258.0 ± 9.5 mm² when the pneumatic pressure (p_a) ranged from 20 kPa to 140 kPa (Fig. 2h, blue diamonds). The average chamber area at the maximum pneumatic pressure (before the rupture of the film) was smaller than μ PAC with $E = 169.4$ kPa (354.1 ± 100.5 mm², Fig. 2h, green triangle). This result indicated that the reduced Young's modulus of the film increased the maximum pneumatic pressure that could be withheld without rupturing. Previous research verified that the soft thin film (Ecoflex 00-10) could withstand more strain than the hard thin film (Ecoflex 00-50).⁵⁶ The bending angle ranged from $\theta = 2.1 \pm 2.1^\circ$ ($P_a = 20$ kPa) to $\theta = 72.2 \pm 10.4^\circ$ ($P_a = 140$ kPa,

Fig. 2i, blue diamonds). The bending angles of μPAC with $E = 41$ kPa were approximately the same as μPAC with $E = 169.4$ kPa when the average chamber area was approximately the same; for example, $\theta = 39.7 \pm 7.0^\circ$ ($E = 41$ kPa, $A = 147.5 \pm 47.0$ mm², $P_a = 110$ kPa) and $\theta = 37.6 \pm 17.7^\circ$ ($E = 169.4$ kPa, $A = 150.5 \pm 59.8$ mm², $P_a = 60$ kPa) were comparable (Fig. S4a†). Overall, the range of the bending angle was comparable regardless of two Young's modulus of the thin film ($E = 41$ kPa and 169.4 kPa) we studied, while the higher pneumatic pressure was required to achieve the same bending angles for the actuator with the lower Young's modulus. When changing the thickness (t) and the chamber length (L), the expansion and bending behavior of μPAC ($E = 41$ kPa) exhibited similar trends to those with the high Young's modulus ($E = 169.4$ kPa) (details in ESI† S4, Fig. S4b).

Overall, this study identified three major parameters—(1) the thickness of the silicon thin film, (2) the chamber size, and (3) Young's modulus of the silicone thin film—to control the expansion and bending behaviors of μPAC . The thickness of the silicone thin film and Young's modulus largely influenced the range of the pneumatic pressure that the μPAC could withstand. μPAC fabricated with the thicker or softer film could withstand the larger pressure, while the higher pressure was required to expand the pneumatic chamber. The bending angle was determined by the chamber area, and it is thus possible to change its responsiveness to pneumatic pressure by changing the thickness and Young's modulus. Other parameters, such as the distance between adjacent pneumatic chambers and the mechanical properties of the cellulose paper (e.g., thickness and pore size), would influence the bending behaviors. Lastly, creating proper contact between pneumatic chambers is critical to achieving the actuation, and the design of the pneumatic chamber (e.g., a circle-shaped chamber, triangle-shaped chamber, and parallelogram-shaped chamber) should induce complex patterns of actuation, which is left for further investigation.

When enlarging the chamber size, the imbalance of expansion occurred between the front chamber and the back chambers, resulting in the small bending angle of μPAC at the low pneumatic pressure. We believe this asymmetry of the expansion can be attributed to the design of the chambers; the front chamber is anchored by three sides by the silicone sealant (with one side having the airpath) while the back chamber is anchored by two sides by the silicone sealants (with two sides having the airpath). This difference in the geometry of the chambers caused the back chamber more prone to expand than the front chamber when the same pressure was applied simultaneously.

3.2. Repeated actuation of the thin-film soft-actuator

To characterize the performance of μPAC , we considered two types of repeatability in this study: (1) the repeatability of the bending performance of the pneumatic soft actuator and (2) the reusability of the integrated paper-based sensor. We first observed the repeatability of the actuation of μPAC by cyclic

application of pressure, $p_a = 100$ kPa with intervals of 5 s (Movie S1†). The pneumatic chamber expanded immediately as the pressure was applied, and the bending angle (θ) was gradually increased from 62° (1 s) to 79° (5 s) while the pressure was applied (Fig. 3a and b). The pneumatic chamber deflated as soon as the applied pressure was stopped, and the bending angle (θ) decreased to 21° (10 s). The deformation of the cellulose paper was not completely reverted to the initial straight state. The actuations were performed five times, and a gradual increase in bending angle was observed after each cycle.

3.3. μPAC as a soft gripper

We designed μPAC with five pneumatic chambers to demonstrate gripping like an octopus arm (Fig. 3c). The chamber length was 7.5 mm, and the interval of chambers was 2 mm. When applying 200 kPa to the μPAC with five pneumatic chambers, all chambers were successfully expanded (Fig. 3d). These results showed that μPAC can be actuated with an increased number of chambers. In this experiment, the bending angle of the pneumatic chamber having pneumatic microchannels on both sides (Point 2 and Point 3) was larger than the pneumatic chamber with one side closed (Point 4). This observation indicated that the configuration and the arrangement of the pneumatic chamber influenced the bending behavior (details in ESI† S5, Fig. S5). To demonstrate the gripping motion, μPAC with five pneumatic chambers was actuated to catch a tube (6.7 g weight) by applying a constant pressure ($p_a = 200$ kPa). μPAC with five pneumatic chambers wrapped the side of the tube and held the tube while lifted (Fig. 3e). This result indicated that μPAC can be potentially used as a soft, pneumatic gripper with a flexible design of gripping arms.

The presence of multiple chambers allows complex motion of μPAC , demonstrating wrapping, gripping, and grasping with 360° of rotation (details in ESI† S6, Fig. S6). The chambers can be designed in two dimensions to achieve motions on more than two planes (Fig. S6b and d†). We believe complex motions, such as hand-like motion with multiple fingers with independent motions, and actuation that conforms to curved surfaces, can be achieved using the design of the actuators that we presented. For applying μPAC to conventional robotics, it is essential to characterize the forces generated by the actuator. Detailed characterization of the forces generated by different designs of μPAC is under current investigation.

3.4. Paper-based microfluidic colorimetric chemical sensor integrated soft μPAC

Finally, we demonstrated that μPAC was applied to perform chemical sensing during the actuation. To demonstrate the principle, we performed pH sensing of a spherical-shaped target by creating a conformal contact along the surface of the target objects. To fabricate the pH sensor, molten paraffin wax was circularly printed (diameter 4 mm) on the cellulose paper

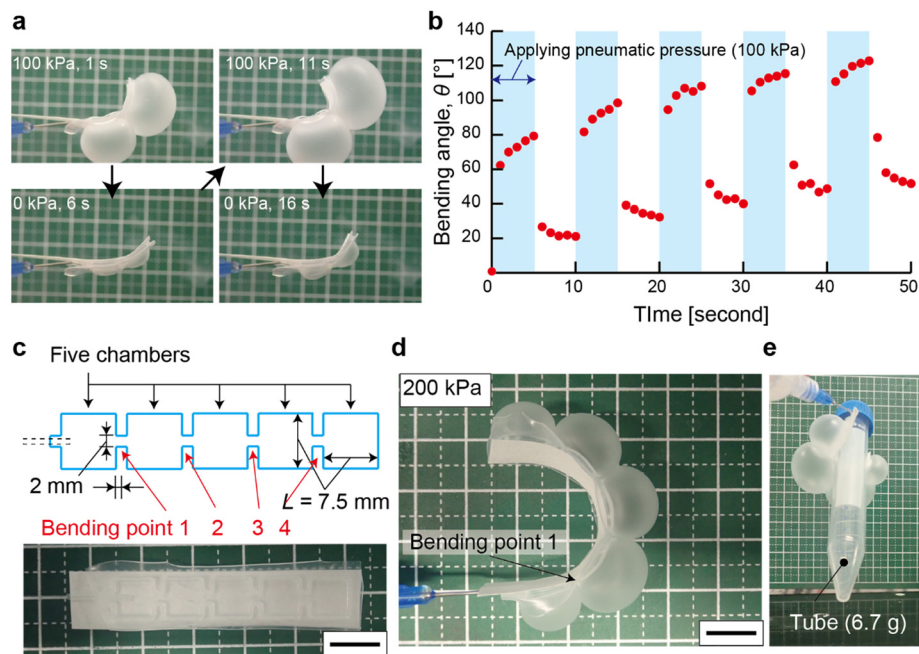


Fig. 3 Demonstration of μ PAC. (a) Photographs showing repeated actuation of μ PAC. (b) Plot showing the bending angle of μ PAC (θ) over time, with repeated actuation. (c) Design and photograph of μ PAC with five pneumatic chambers. (d) Photograph showing the bending of μ PAC with five pneumatic chambers. (e) Photograph showing the gripping of a test tube by μ PAC with five pneumatic chambers. Scale bars: 10 mm.

substrate (Fig. 4a, top). The printed wax vertically penetrated through the cellulose paper, which would inhibit the mechanical interlocking between the cellulose paper and the silicone sealant. As such, it is crucial to avoid overlapping the print path of the wax with the print path of the silicone sealant. The printed paraffin wax served as a hydrophobic barrier to confine the pH indicator. The color of the pH indicator changed in response to the pH, and thus the pH of the target samples can be estimated using the hue value of the indicator (details in ESI† S7, Fig. S7). After fabricating two colorimetric pH sensors on the cellulose paper, the cellulose paper substrate was integrated into the soft actuator ($L = 7.5$ mm, $t = 1.8$ mm, and $E = 169.4$ kPa) (Fig. 4a, bottom). μ PAC with colorimetric pH sensors was designed to test the top (region A) and the side (region B) of the spherical object simultaneously (Fig. 4b). A small lime was used as the sensing target; the damage on the surface caused reduced pH due to the seeping of the acidic juice (Fig. 4c). Three target samples—a non-damaged sample, an entirely damaged sample, and a partially damaged sample—were prepared to perform experiments with an appropriate control (Table 1). The pH indicator used in this experiment underwent a color change to red when the pH was below 3. The ratio of red to green values in the RGB spectrum (V_r and V_g) was measured before and after sensing, and the ratio of the change (R_c) was calculated to quantify the color change as in eqn (1).

$$R_c = \frac{V_{r,\text{after}}/V_{g,\text{after}}}{V_{r,\text{before}}/V_{g,\text{before}}} \quad (1)$$

When the pH-sensing μ PAC was placed on the target sample without applying pneumatic pressure, the sensor contacted only with the top surface of the sample (Fig. 4d, top). The pH-sensing

μ PAC made a conformal contact with the surface of the target by applying pressure, allowing the sensing regions to contact with the surface of the lime (Fig. 4d, bottom, Movie S2†). When sensing the non-damaged surface (sample 1), the color of the pH sensors remained green after contacting the top and side surfaces (Fig. 4e, top, Fig. S8a† yellow bars). In contrast, when sensing the entirely damaged surface (sample 2), the color of both pH sensors was changed from green to red due to the acidic juice of the lime from the damage (Fig. 4e, middle, Fig. S8a† pink bars). The pH-sensing μ PAC was used to test the partially damaged sample surface (sample 3). The color of the pH sensor on the side was green before actuation (Fig. 4e, bottom) and red after actuation (Fig. 4e, bottom). These results demonstrated that the pH-sensing μ PAC successfully detected the damaged areas of the target samples by forming conformal contact with the curved target sample. The color change occurred immediately after absorbing the aqueous sample (1.5 s), suggesting that the response rate was largely limited by the diffusion of the aqueous sample (*i.e.*, acidic juice) to the sensing region (ESI† S9, Fig. S9). The actuation was crucial to ensure the contact of the sensing regions with the curved surface. μ PAC successfully maintained the curved shape along the lime even after absorbing the acidic juice released from the damage of the target sample (ESI† S9, Fig. S9). These observations suggested that μ PAC was in contact with the surface of wet samples and successfully measured the surface condition of the target sample. Lastly, the color change ratio (R_c) of the sensing non-damaged surface and the damaged sample were 1.02 ± 0.006 and 1.14 ± 0.060 , respectively (Fig. 4f). Overall, the pH-sensing μ PAC successfully demonstrated the detection of the damaged region of the spherical line surface by actuating the device.

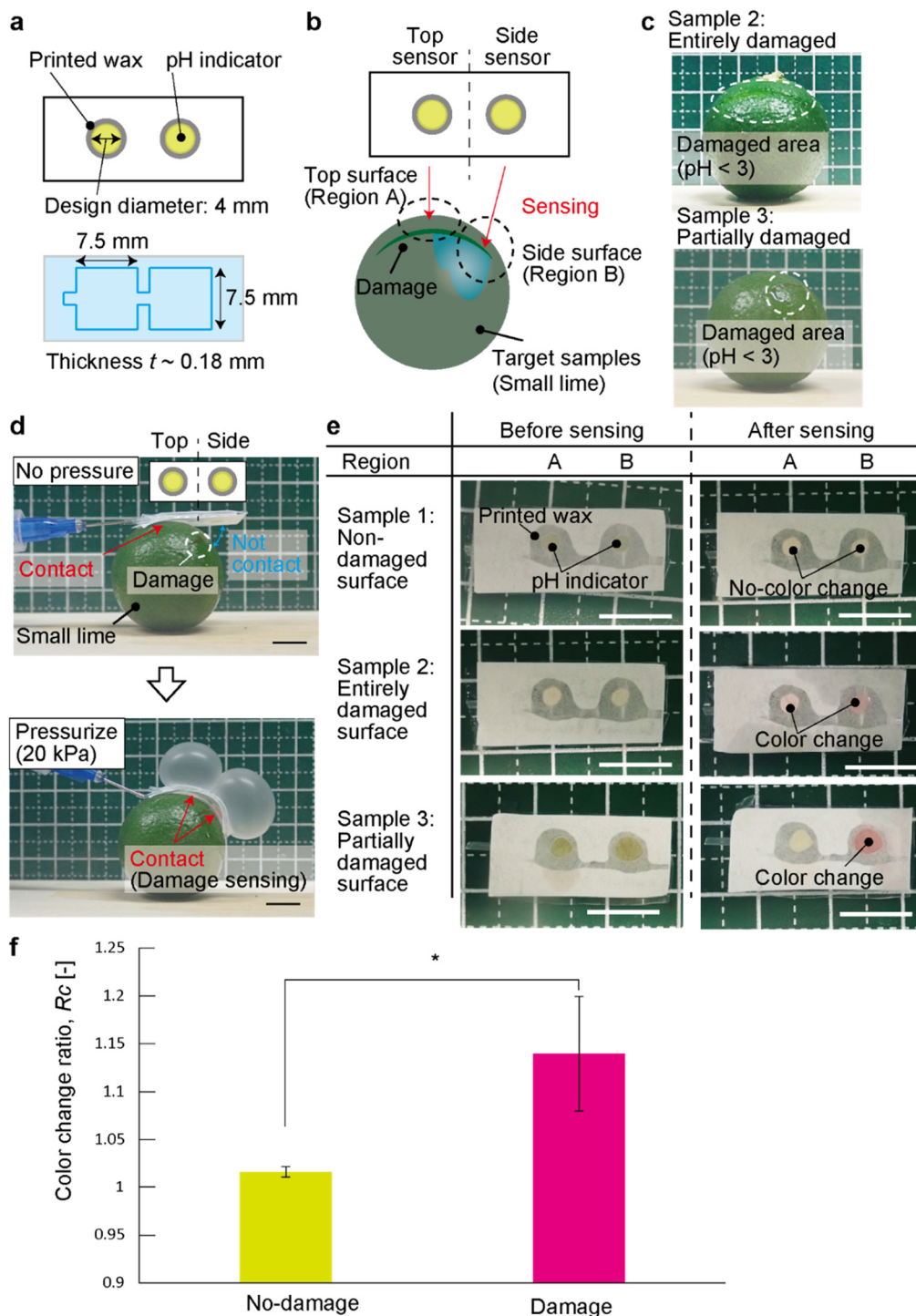


Fig. 4 pH sensing with μ PAC. (a) Illustration of colorimetric pH sensors integrated with μ PAC. (b) Illustration of the application of pH-sensing μ PAC on a small lime sample. (c) Photographs of the entirely damaged target (sample 2) and the partially damaged target (sample 3). (d) Photographs showing the application of μ PAC on a lime sample. Application of the pressure allows the actuation of the sensing region to the detection area of the sample. (e) Photographs showing the color change of three samples (samples 1, 2, 3). (f) Plot showing the color change ratio (R_c) comparing the detection of the non-damaged and damaged surfaces. The asterisk (*) indicates a significant difference observed in a one-sided t -test ($t < 0.05$). The scale bars: 10 mm.

This demonstration suggested that μ PAC enabled spatially-resolved chemical sensing on the curved surface by actuation. Altering the design of the pneumatic chambers makes it possible to tailor the motion of the soft actuators for intended

applications. Silicone-based (or polymer-based) soft actuators exhibit selected chemical resistance compared to metal-based actuators (such as acid–base and reduction–oxidation reactions). With the realization of low-cost, single-use actuators

Table 1 The conditions of the target samples

	Region	
	A	B
Sample 1: Non-damaged sample	Undamaged	Undamaged
Sample 2: Entirely damaged sample	Damaged	Damaged
Sample 3: Partially damaged sample	Undamaged	Damaged

equipped with chemical sensors, emerging applications such as simultaneous detection of food spoilage while sample collection would be possible. The capability to actuate the sensing region of the device would be potentially beneficial to ensure proper collection of the testing samples when remote operation is needed. To this end, our demonstration employed a pH indicator exhibiting discernible color changes upon the change in pH. Using the same platform, it is possible to embed other types of colorimetric inks to alter the sensing capability. For example, a paper-based temperature sensor was readily developed with thermochromic ink, which displayed pronounced color changes with observable differences (hue = 214.5 and 344.5) (ESI† S10, Fig. S10). Appropriate selection of colorimetric reagents is critical for successful chemical sensing tailored to specific applications.

We note that the repeated use of μ PAC (*i.e.*, the reusability) was not demonstrated in this work because the pneumatic actuator was directly integrated with the paper-based sensing region. In the current design, the cellulose paper serves for dual purpose: (1) the substrate to perform chemical sensing, and (2) the strain-limiting layer to bend the soft actuator. Similarly to μ PAD, the sensor was meant to be disposable and used only one time. The reusability of μ PAC would require a different device design that allows the separation of the sensor from the actuator. Alternatively, the complete washing to remove the reagents and the samples from the paper substrate may facilitate the repeated usage of μ PAC. However, the feasibility would depend on the nature of the sensing reaction performed on μ PAC. Nevertheless, because the cellulose paper and the silicone elastomer are readily available at low cost, the current design of μ PAC would be suitable for a one-time sensor.

Conclusions

In this research, we demonstrated the concept of the thin-film soft actuator integrated with a paper-based chemical sensor, termed a microfluidic paper-based analytical soft actuator (μ PAC). A cellulose paper in μ PAC serves dual purposes: (1) strain-limiting layer of the soft actuator, and (2) porous substrate to hold analytical reagents for chemical sensing. μ PAC ($t = 0.40$ mm, $L = 7.5$ mm, and $E = 169.4$ kPa) exhibited the bending motion with $\theta = 87.0 \pm 7.8^\circ$ by applying pneumatic pressure ($p_a = 110$ kPa), where the bending angle was readily controlled with the applied pressure. We identified that the thickness and Young's modulus of the elastomeric thin film are major variables to control the

expansion of the pneumatic chamber. μ PAC can be designed to perform gripping motion (holding a tube with 6.7 g weight). Lastly, pH detection on a spherical surface was demonstrated by integrating pH sensing reagents with μ PAC. The actuation of μ PAC allowed conformal contact of the paper-based substrate with the curved surface of the sample, allowing pH detection at different locations of the spherical sample simultaneously.

μ PAC offers distinct advantages over conventional soft actuators. First, μ PAC can be readily fabricated by DIW printing with low-cost materials. DIW printing allows the printing of various materials (*e.g.*, silicone sealant and paraffin wax) on different substrates (*e.g.*, cellulose papers and polymer films), which is suitable for rapid prototyping. The mode of actuation (such as gripping, grasping, and wrapping) can be readily tailored by the design of the printed microchambers. Integration of actuators with chemical sensors opens up a myriad of applications in agriculture, environmental sensing and healthcare. The capability to actuate the sensing region of the analytical device may benefit in scenarios where the simultaneous collection of the samples is necessary at different locations. We believe that μ PAC paves an avenue for designing paper-based analytical devices with unprecedented usage that requires actuation of the chemical sensors.

Experimental section/materials and methods

Materials. Paraffin wax (327212, Sigma-Aldrich, Singapore), poly(vinylalcohol) 500 (32283-02, Kanto Kagaku, Japan), a fast-curing silicone sealant (wet area SPEEDSEAL silicone, Selleys, Sydney, Australia), Ecoflex 00-10 (Smooth-On Inc., Pennsylvania, USA), Ecoflex 00-30 (Smooth-On Inc., Pennsylvania, USA) were used as purchased. The cellulose paper (Grade 1, Whatman, Sigma-Aldrich, Singapore) was used as a substrate of μ PAC.

Fabrication of the μ PAC. Ecoflex films were created by spin-coating or molding. To easily remove Ecoflex thin film, a glass slide coated with 10% (w/w) polyvinyl alcohol (PVA, 32283-02, Kanto Kagaku, Tokyo, Japan) was used as a substrate. Spin-coating was performed at 300 rpm for 60 s for the mixed resin of Ecoflex. To cast Ecoflex, a mold was prepared using a glass plate (S9213, Matsunami Glass Ind., Ltd., Osaka, Japan) and silicone-based double-sided tape (No. 7082, Teraoka Seisakusyo Co., Ltd., Tokyo, Japan). To achieve a thickness of ~ 0.4 mm, four layers of double-sided tape were stacked. The four-layered tape was applied along each of the four edges of the glass plate, creating a frame with a height of ~ 0.4 mm. Ecoflex was poured into the frame, and excess Ecoflex was removed using another glass plate. After the spin coating or molding, the Ecoflex film was cured at 120 °C over 2 h. The thickness of the created Ecoflex film was measured using a calliper. The range of the thickness was 0.17 mm to 0.41 mm.

The silicone sealant was filled with the syringe (PSY-50F, Musashi Engineering Inc., Tokyo, Japan) and printed by using a commercially available liquid dispenser (SHOT MASTER 500

ΩX, Musashi Engineering Inc., Tokyo, Japan) through a 22 G plastic nozzle (Birmingham Gauge) (V-S Liquid control equipment, China). The syringe filled with the silicone sealant, the plastic nozzle, and the liquid dispenser were maintained at room temperature. Four layers of the silicone sealant were printed on the Ecoflex film. After printing the silicone sealant, a silicone tube (SR-1554, ARAM Corporation, Osaka, Japan) was placed on the edge of the pneumatic chamber as an inlet of air. Then the additional silicone sealant was printed on the tube. The cellulose paper (Grade 1, Whatman, Sigma-Aldrich, Singapore) was placed on the printed silicone sealant. The printed silicone sealant was cured overnight. The printing toolpath was designed by MuCAD (Musashi Engineering Inc., Tokyo, Japan).

Actuation of the μ PAC. The fabricated μ PAC was connected to the syringe *via* the 22 G needle nozzle (Yueqing Huhang Electric Co., Ltd., Yueqing City, China). The pneumatic pressure was applied through the pneumatic controller (ML-808GX, Musashi Engineering Inc., Tokyo, Japan). The images of the bending behaviors of μ PAC were taken by a compact digital camera (Tough TG-5, Olympus, Tokyo, Japan). The bending angle of the μ PAC was analyzed by ImageJ.

μ PAC ($L = 7.5$ mm, $t = 0.17$ mm) was fabricated with Ecoflex 00-10 thin film for repeated actuation. The pneumatic pressure of 100 kPa was applied at a five-second interval. The movie showing the actuation of μ PAC was taken by the compact digital camera, and then the images were captured from the movie every second. The bending angle, θ , was measured every second by using ImageJ.

Gripping object by μ PAC. We fabricated the μ PAC with five pneumatic chambers using Ecoflex 00-10 thin film ($L = 7.5$ mm, $t = 0.17$ mm). The pneumatic pressure ($p_a = 200$ kPa) was applied to the μ PAC with five pneumatic chambers. To demonstrate the gripping application, a tube (weight: 6.7 g) was used as a target sample.

Fabrication of colorimetric chemical sensor. Paraffin wax was filled with the syringe. A metal nozzle (inner diameter: 0.1 mm, SHN-0.1 N, Musashi Engineering Inc., Tokyo, Japan) was connected to the syringe. The syringe was heated by a syringe heater (100 °C, TB-50E-K, Musashi Engineering Inc., Tokyo, Japan) controlled by a heater controller (TCU-02-MU, Musashi Engineering Inc., Tokyo, Japan) for melting the paraffin wax. Before printing the paraffin wax, the nozzle was additionally heated by a heater gun (150 °C, HG6530V, Makita Corporation, Aichi, Japan). The molten paraffin wax was printed in a circular shape on the cellulose paper (platform temperature: 35 °C) using the liquid dispenser. The toolpath was designed by MuCAD. The pH indicator (DM-2, Takemura Denki Seisakusho, Tokyo, Japan) was infiltrated in the circular region defined by the printed wax just before the sensing target to prevent it from drying out. This design prevents the color sensor ink from diffusing around the target when detecting the object. The pH indicator changes its color between pH = 4 and pH = 10, containing a mixture of ethylene glycol, ethanol, sodium hydroxide, methyl orange, phenolphthalein, methyl red, bromothymol blue, and water.

Local pH sensing. μ PAC was constructed using two circular printed paraffin waxes on the cellulose paper, with a pH indicator confined in the circular regions defined by the printed wax. Small limes (diameter ~ 33 mm) were purchased from a local supermarket. Three detection targets were created by damaging the small limes with a knife. (1) without damage, (2) with the damage on the top and the side, and (3) with the damage on the side. To actuate pH-sensing μ PAC, the pneumatic pressure with the range of 20–60 kPa was applied. The color of the chemical sensor was divided into RGB channels by ImageJ (Function of RGB stack). The gray values of R and G channels (V_r and V_g) were then measured by ImageJ. The ratio of the red value to the green value in the RGB spectrum was calculated before and after sensing. The ratio of this change (color change ratio, R_c) was calculated as a measure of the color change by using Excel (Microsoft, Washington, USA).

Data availability

The data that support the findings of this study are available from the corresponding author upon reasonable request.

Conflicts of interest

There are no conflicts to declare.

Acknowledgements

K. Y. acknowledges the Research Fellowship for Young Scientists PD (22J01492) and Grant-in-Aid for Early-Career Scientists (23K13289), Japan Society for the Promotion of Science (JSPS), JAPAN. M. H. acknowledges Digital Manufacturing and Design (DManD) Centre at the Singapore University of Technology and Design (RGDM1620403), Agency for Science, Technology, and Research (A*STAR) (M22K2c0085), and Ministry of Education (MOE), Singapore (Academic Research Fund (AcRF) Tier 2, MOE-T2EP50122-0025) for the project funding.

References

- 1 J. Kim, J. W. Kim, H. C. Kim, L. Zhai, H. U. Ko and R. M. Muthoka, *Int. J. Precis. Eng. Manuf.*, 2019, **20**, 2221–2241.
- 2 D. Rus and M. T. Tolley, *Nature*, 2015, **521**, 467–475.
- 3 C. Laschi, B. Mazzolai and M. Cianchetti, *Sci. Robot.*, 2016, **1**(1), 1–11.
- 4 P. Won, K. K. Kim, H. Kim, J. J. Park, I. Ha, J. Shin, J. Jung, H. Cho, J. Kwon, H. Lee and S. H. Ko, *Adv. Mater.*, 2021, **33**(19), 1–19, 2002397.
- 5 S. I. Rich, R. J. Wood and C. Majidi, *Nat. Electron.*, 2018, **1**, 102–112.
- 6 K. Yoshida, S. Nakajima, R. Kawano and H. Onoe, *Sens. Actuators, B*, 2018, **272**, 361–368.
- 7 Y. Takashima, S. Hatanaka, M. Otsubo, M. Nakahata, T. Kakuta, A. Hashidzume, H. Yamaguchi and A. Harada, *Nat. Commun.*, 2012, **3**(1270), 1–8.

- 8 B. Mosadegh, P. Polygerinos, C. Keplinger, S. Wennstedt, R. F. Shepherd, U. Gupta, J. Shim, K. Bertoldi, C. J. Walsh and G. M. Whitesides, *Adv. Funct. Mater.*, 2014, **24**(15), 2163–2170.
- 9 E. Acome, S. K. Mitchell, T. G. Morrissey, M. B. Emmett, C. Benjamin, M. King, M. Radakovitz and C. Keplinger, *Science*, 2018, **359**(6371), 61–65.
- 10 V. Caccucciolo, J. Shintake, Y. Kuwajima, S. Maeda, D. Floreano and H. Shea, *Nature*, 2019, **572**, 516–519.
- 11 P. Polygerinos, N. Correll, S. A. Morin, B. Mosadegh, C. D. Onal, K. Petersen, M. Cianchetti, M. T. Tolley and R. F. Shepherd, *Adv. Eng. Mater.*, 2017, **19**(12), 1–22, 1700016.
- 12 M. S. Xavier, C. D. Tawk, A. Zolfagharian, J. Pinski, D. Howard, T. Young, J. Lai, S. M. Harrison, Y. K. Yong, M. Bodaghi and A. J. Fleming, *IEEE Access*, 2022, **10**, 59442–59485.
- 13 B. Gorissen, D. Reynaerts, S. Konishi, K. Yoshida, J. W. Kim and M. De Volder, *Adv. Mater.*, 2017, **29**(43), 1–14, 1604977.
- 14 T. H. Yang, J. Shintake, R. Kanno, C. R. Kao and J. Mizuno, *Adv. Intell. Syst.*, 2020, **2**(8), 1–7, 2000025.
- 15 M. Schaffner, J. A. Faber, L. Pianegonda, P. A. Rühls, F. Coulter and A. R. Studart, *Nat. Commun.*, 2018, **9**(878), 1–9.
- 16 R. F. Shepherd, F. Ilievski, W. Choi, S. A. Morin, A. A. Stokes, A. D. Mazzeo, X. Chen, M. Wang and G. M. Whitesides, *Proc. Natl. Acad. Sci. U. S. A.*, 2011, **108**(51), 20400–20403.
- 17 R. V. Martinez, C. R. Fish, X. Chen and G. M. Whitesides, *Adv. Funct. Mater.*, 2012, **22**(7), 1376–1384.
- 18 R. F. Shepherd, A. A. Stokes, R. M. D. Nunes and G. M. Whitesides, *Adv. Mater.*, 2013, **25**(46), 6709–6713.
- 19 A. Yamaguchi, K. Takemura, S. Yokota and K. Edamura, *Sens. Actuators, A*, 2011, **170**(1–2), 139–146.
- 20 A. Heiden, D. Preninger, L. Lehner, M. Baumgartner, M. Drack, E. Woritzka, D. Schiller, R. Gerstmayr, F. Hartmann and M. Kaltenbrunner, *Sci. Robot.*, 2022, **7**(63), 1–10, eabk2119.
- 21 A. A. Amiri Moghadam, S. Alaie, S. Deb Nath, M. Aghasizade Shaarba, J. K. Min, S. Dunham and B. Mosadegh, *Soft Robot.*, 2018, **5**(4), 443–451.
- 22 V. Sanchez, K. Mahadevan, G. Ohlson, M. A. Graule, M. C. Yuen, C. B. Teeple, J. C. Weaver, J. McCann, K. Bertoldi and R. J. Wood, *Adv. Funct. Mater.*, 2023, **33**(26), 1–12, 2212541.
- 23 Y. Hori and S. Konishi, *Microsyst. Nanoeng.*, 2023, **9**(55), 1–12.
- 24 S. Russo, T. Ranzani, C. J. Walsh and R. J. Wood, *Adv. Mater. Technol.*, 2017, **2**(10), 1–12, 1700135.
- 25 B. Gorissen, D. Reynaerts, S. Konishi, K. Yoshida, J. W. Kim and M. De Volder, *Adv. Mater.*, 2017, **29**(43), 1–14, 1604977.
- 26 B. Gorissen, T. Chishiro, S. Shimomura, D. Reynaerts, M. De Volder and S. Konishi, *Sens. Actuators, A*, 2014, **216**, 426–431.
- 27 B. Mosadegh, P. Polygerinos, C. Keplinger, S. Wennstedt, R. F. Shepherd, U. Gupta, J. Shim, K. Bertoldi, C. J. Walsh and G. M. Whitesides, *Adv. Funct. Mater.*, 2014, **24**(15), 2163–2170.
- 28 T. Ching, Y. Li, R. Karyappa, A. Ohno, Y. C. Toh and M. Hashimoto, *Sens. Actuators, B*, 2019, **297**(126609), 1–9.
- 29 K. Yamagishi, T. Ching, N. Chian, M. Tan, W. Zhou, S. Y. Huang and M. Hashimoto, *Adv. Funct. Mater.*, 2023, **34**(31), 1–11, 2311219.
- 30 K. Yamagishi, W. Zhou, T. Ching, S. Y. Huang and M. Hashimoto, *Adv. Mat.*, 2021, **33**(26), 1–15, 2008062.
- 31 M. Wehner, R. L. Truby, D. J. Fitzgerald, B. Mosadegh, G. M. Whitesides, J. A. Lewis and R. J. Wood, *Nature*, 2016, **536**, 451–455.
- 32 W. Wu, A. Deconinck and J. A. Lewis, *Adv. Mat.*, 2011, **23**(24), 178–183.
- 33 Y. F. Zhang, C. J. X. Ng, Z. Chen, W. Zhang, S. Panjwani, K. Kowsari, H. Y. Yang and Q. Ge, *Adv. Mater. Technol.*, 2019, **4**(10), 1–9, 1900427.
- 34 P. Zhou, J. Lin, W. Zhang, Z. Luo and L. Chen, *Nano Res.*, 2022, **15**(6), 5376–5383.
- 35 L. Chen, M. Weng, P. Zhou, F. Huang, C. Liu, S. Fan and W. Zhang, *Adv. Funct. Mater.*, 2019, **29**(5), 1–9, 1806057.
- 36 J. Chen, K. Han, J. Luo, L. Xu, W. Tang and Z. L. Wang, *Nano Energy*, 2022, **70**(105171), 1–8.
- 37 H. Zhao, K. O'Brien, S. Li and R. F. Shepherd, *Sci. Robot.*, 2016, **1**(1), 1–10, eaai7529.
- 38 R. L. Truby, M. Wehner, A. K. Grosskopf, D. M. Vogt, S. G. M. Uzel, R. J. Wood and J. A. Lewis, *Adv. Mat.*, 2018, **30**(15), 1–8, 1706383.
- 39 K. B. Justus, T. Hellebrekers, D. D. Lewis, A. Wood, C. Ingham, C. Majidi, P. R. Leduc and C. Tan, *Sci. Robot.*, 2019, **4**(31), 1–7.
- 40 C. Xu, Y. Song, J. R. Sempionatto, S. A. Solomon, Y. Yu, H. Y. Y. Nyein, R. Y. Tay, J. Li, W. Heng, J. Min, A. Lao, T. K. Hsiai, J. A. Sumner and W. Gao, *Nat. Electron.*, 2024, **7**, 168–179.
- 41 Z. Xiong, S. Achavananthadith, S. Lian, L. Edward Madden, Z. Xin Ong, W. Chua, V. Kalidasan, Z. Li, Z. Liu, P. Singh, H. Yang, S. P. Heussler, S. M. P. Kalaiselvi, M. B. H. Breese, H. Yao, Y. Gao, K. Sanmugam, B. C. K. Tee, P.-Y. Chen, W. Loke, C. Teck Lim, G. S. H. Chiang, B. Y. Tan, H. Li, D. L. Becker and J. S. Ho, *Sci. Adv.*, 2021, **7**(47), 1–11, eabj1617.
- 42 Y. Yu, J. Li, S. A. Solomon, J. Min, J. Tu, W. Guo, C. Xu, Y. Song and W. Gao, *Sci. Robot.*, 2022, **7**(67), 1–12, eabn0495.
- 43 D. Kim, Y. Cao, D. Mariappan, M. S. Bono, A. J. Hart and B. Marelli, *Adv. Funct. Mater.*, 2021, **31**(1), 1–9, 2005370.
- 44 K. Yamada, H. Shibata, K. Suzuki and D. Citterio, *Lab Chip*, 2017, **17**(7), 1206–1249.
- 45 J. S. Ng and M. Hashimoto, *RSC Adv.*, 2020, **10**(50), 29797–29807.
- 46 E. Carrilho, A. W. Martinez and G. M. Whitesides, *Anal. Chem.*, 2009, **81**(16), 7091–7095.
- 47 Y. Yamanaka, S. Katagiri, H. Nabae, K. Suzumori and G. Endo, *Proceedings of the 2020 IEEE/SICE*, 2020, 87–92.
- 48 Y. Liu, J. Hou, C. Li and X. Wang, *Adv. Intell. Syst.*, 2023, **5**(12), 1–30, 2300233.
- 49 R. K. Mishra, L. J. Hubble, A. Martin, R. Kumar, A. Barfidokht, J. Kim, M. M. Musameh, I. L. Kyratzis and J. Wang, *ACS Sens.*, 2017, **2**(4), 553–561.
- 50 S. Russo, T. Ranzani, C. J. Walsh and R. J. Wood, *Adv. Mater. Technol.*, 2017, **2**(10), 1–12, 1700135.

- 51 T. Ching, J. Lee, S. Win, L. Win, D. Sufiyan, C. Lim, N. Nagaraju, Y. Toh, S. Foong and M. Hashimoto, *Sci. Robot.*, 2024, **9**(92), 1–13, eadk4533.
- 52 E. Aucone, S. Kirchgeorg, A. Valentini, L. Pellissier, K. Deiner and S. Mitchev, *Sci. Robot.*, 2023, **8**(74), 1–13, eadd5762.
- 53 T. Ching, Y. Li, R. Karyappa, A. Ohno, Y. C. Toh and M. Hashimoto, *Sens. Actuators, B*, 2019, **297**(126609), 1–9.
- 54 S. Zhao, C. C. Nguyen, T. T. Hoang, T. N. Do and H. P. Phan, *Sensors*, 2023, **23**(12), 1–14.
- 55 A. Atieh, Design, Modeling, Fabrication and Testing of a Piezoresistive-Based Tactile Sensor for Minimally Invasive Surgery Applications, *Master's Thesis*, Concordia University, 2012.
- 56 Z. Liao, M. Hossain and X. Yao, *Mech. Mater.*, 2020, **144**(103366), 1–12.